

# A Comparison of Deep HST Luminosity Functions of Four Globular Clusters<sup>1</sup>

Giampaolo Piotto<sup>2</sup>, Adrienne M. Cool<sup>3</sup>, and Ivan R. King<sup>4</sup>

Received \_\_\_\_\_; accepted \_\_\_\_\_

---

<sup>1</sup>Based on observations with the NASA/ESA *Hubble Space Telescope*, obtained at the Space Telescope Science Institute, which is operated by AURA, Inc., under NASA contract NAS5-26555

<sup>2</sup>Dipartimento di Astronomia, Università di Padova, Vicolo dell’Osservatorio 5, I-35122 Padova, Italy

<sup>3</sup>Astronomy Department, University of California, Berkeley, CA 94720-3411, and Department of Physics and Astronomy, San Francisco State University, 1600 Holloway Avenue, San Francisco, CA 94132

<sup>4</sup>Astronomy Department, University of California, Berkeley, CA 94720-3411

## ABSTRACT

From deep color–magnitude arrays made from  $V$  and  $I$  images taken with *Hubble Space Telescope*’s WFPC2 camera we have determined luminosity functions (LFs) down to a level that corresponds to  $\sim 0.13 M_{\odot}$ , for the low-metal-abundance globular clusters M15, M30, M92, and NGC 6397. Because of the similarity of the metallicities of these clusters, differences in their luminosity functions directly trace differences in their mass functions. The LFs of M15, M30, and M92 agree closely over the entire observed range, whereas that of NGC 6397 drops away sharply at the faintest magnitudes. We suggest that the deficiency of low-mass stars in NGC 6397 is due to tidal shocks, to ejection through internal relaxation, or to a combination of the two. With the presently available mass–luminosity relations, we find that even in M15, M30, and M92 the mass functions probably do not rise so fast as to make the low-mass end dominant.

*Subject headings:* Globular clusters: individual (NGC 6397, M15, M30, M92); stars: low-mass — luminosity function

## 1. Introduction

The *Hubble Space Telescope (HST)* now makes it possible to derive color–magnitude diagrams (CMDs) of globular clusters (GCs) that extend several magnitudes fainter than the CMDs found for the same clusters from the ground. Among the important by-products of these CMDs are luminosity functions (LFs), and from them mass functions (MFs), that can extend over nearly the entire length of the lower main sequence.

Insight into the formation and dynamical evolution of globulars can be gained by using these LFs and MFs to compare the stellar content of different clusters. It has often been suggested that the mass function of a cluster depends on its position in the Galaxy, its metallicity, and its dynamical history (see, e.g., McClure *et al.* 1986, Aguilar, Hut, & Ostriker 1989, Djorgovski, Piotto, & Capaccioli 1993); and the relationships are complicated by the fact that the latter two factors correlate with the first. In any case, the main-sequence mass functions of clusters are one of our important clues relating to their origin.

Furthermore, globular clusters have quite often been used as tracers and indicators of the halo population of which they are the most conspicuous part. In particular, it has been suggested that there is a steep rise at the low-mass end of cluster MFs (Richer *et al.* 1991), and that this might be indicative of a considerable contribution by low-mass stars to the little-known total mass that governs the poorly understood flat rotation curve of the Galaxy (Richer & Fahlman 1992). In the case of the Galaxy, the steep MF slope that Richer and Fahlman (1992) found at the faint end has been contradicted by better data by Reid *et al.* (1996); and we shall show here that their assertion about steep MFs for low-mass stars in globular clusters also fails to be borne out by improved data that we will present below. Of equal importance will be the demonstration that with one exception that is probably understandable, our sample of clusters shows a remarkable uniformity of mass functions.

Progress on these issues requires accurate photometry of low-mass main-sequence stars. Ground-based studies have so far been limited largely to the mass range above  $0.4\mathcal{M}_\odot$ ; deeper

studies have been pursued only with difficulty and uncertainty. With the advent of *HST*, however, we can largely circumvent the crowding problems that plague ground-based observations, reaching several magnitudes deeper, down to masses close to the bottom end of the hydrogen-burning main sequence.

Here we present the first deep *HST* LFs of M30 (NGC 7099) and M92 (NGC 6341), and independent measurements of the LFs of NGC 6397 and M15 (NGC 7078). The CMD and the LF of NGC 6397 have already been presented in Cool, Piotto, & King (1996, CPK). We compare our results for the latter two clusters with *HST* LFs of Paresce, De Marchi, & Romaniello (1995) and De Marchi & Paresce (1995), and then compare the four cluster LFs with each other. The results of our comparison differ from those reached by De Marchi & Paresce (1995), in that we find a significant difference between the LFs of NGC 6397 and M15.

Two features of this set of four clusters make for a particularly useful comparison. First, three of them have collapsed cores and similar surface-brightness profiles, which make the conversion from the local, observed LFs to global LFs straightforward. M92 is a high-concentration cluster; in this case also the observed LF does not differ appreciably from the global one. Second, all four clusters have comparable metallicities (see Table 1), so that similarities or differences in their LFs will directly reflect similarities or differences in their MFs.

A description of the observations and of the methods of analysis are given in Section 2. We present the cluster LFs and MFs in turn in Sections 3 and 4, exploring in the latter the role of the mass–luminosity relation. The findings are summarized and discussed in Section 5.

## 2. Observations and Analysis

The data were taken with the WFPC2 in parallel mode, in fields  $\sim 4.6'$  from the center of each cluster. (More exactly, the centers of chips W2, W3, and W4 were respectively 5.46, 4.28, and 3.90 arcmin from the center of each cluster, the FOC having been pointed at the cluster center

in every case.) The observation dates and total exposure times are given in Table 1. The NGC 6397 and M30 exposures were obtained with the F814W and F555W filters, and are part of our Cycle-4 observing program. We included short ( $\sim$ 60s) exposures in this program, which allow us to measure stars that were saturated in the long ( $\sim$ 1000s) exposures. The M92 images are part of our Cycle-5 program and were taken with the F814W and F606W filters; short (30s, 100s) exposures were included, making it possible to measure stars up to the turnoff. The choice of the F606W filter, broader than the F555W filter, enabled us to obtain images of nearly matching depth in the two bands with equal exposure times. The M15 exposures, by contrast, came from a generic parallel-exposure program that used the F814W and F606W filters and lacked the short exposures. They are the same images analyzed by De Marchi & Paresce (1995).

Each single long-exposure image was cleaned of cosmic rays using the method described by Anderson, King, & Sosin (1995). Images with identical pointings were averaged. Lists of stars were created for each of the F814W averaged images using DAOPHOT/FIND (Stetson 1987, 1991), modified as described in CPK to help eliminate false detections along diffraction spikes, in the halos of bright stars, and at the positions of hot pixels. The removal of as many of these artifacts as possible was essential for a reliable LF. As in all cases the F814W images were the deepest images, we used the F814W star list for the F555W and F606W images. We measured the magnitudes of the stars using the hybrid weighted, neighbor-subtracted aperture photometry technique described by Cool & King (1995). The first step was to construct a model PSF for each image (using from 100 to 200 stars), consisting of a Moffat function plus residuals, allowing quadratic variation of the residuals with position in the frame. PSF-fitting results from ALLSTAR were then used to subtract all the stars from each image. Next, stars were added back into the “subtracted” image one at a time, reproducing the original data exactly for the added star, but with all the neighbors removed. The flux of each “neighbor-subtracted” star was then measured in an aperture, with the local background estimated using the DAOPHOT routine (Stetson 1987). The aperture magnitude was obtained by weighting each pixel by the reciprocal of its expected variance (Cool & King 1995). The weighted, neighbor-subtracted aperture photometry produced a noticeably tighter main sequence at the faint end than did DAOPHOT used in the conventional way, and the

improvement in photometric accuracy was further confirmed in artificial-star experiments.

We transformed the F814W and F555W instrumental magnitudes into the WFPC2 “ground system” using Eq. 6 of Holtzman *et al.* (1995) and the coefficients in their Table 6. We adopt this photometric system where possible, as it has become the *HST* standard. Hereafter we will refer to these calibrated magnitudes as  $I_{814}$  and  $V_{555}$ . For the range of colors sampled here, the  $I_{814}$  and  $V_{555}$  magnitudes should match  $V$  and  $I$  magnitudes in the Johnson/Cousins system to within a few hundredths of a magnitude (see Fig. 8 in Holtzman *et al.*). As the WFPC2 ground system is not defined for the “wide V” (F606W) filter used to image M92 and M15, we transformed these instrumental magnitudes directly into the “standard” (Johnson/Cousins) system instead, using Eq. 9 and the coefficients in Table 10 of Holtzman *et al.* (1995). Hereafter we refer to these calibrated magnitudes as  $V_{606}$ . For the range of colors sampled in our data,  $V_{606}$  should match Johnson  $V$  to within a few hundredths of a magnitude (see Fig. 10 in Holtzman *et al.*).

In the case of M15 all exposures were aligned, so that we had a single averaged image to work with in each filter. In the case of the other three clusters the fields were not perfectly overlapping and aligned: for NGC 6397 we had 5 averaged images per filter; the number was 3 for M30, and 2 for M92. For each cluster we generated a master list of stars by computing transformations between frames, first correcting for geometrical distortion in the chips, and then requiring that positions agree to within 1.5 pixels (a matching criterion loose enough to avoid selective loss of faint stars). Final magnitudes were derived by flux-averaging the 2 (M92) to 5 (NGC 6397, in the overlapping regions) independent measurements in each filter, so that the full benefit of the information contained in the complete data set was recovered. Note that the CMDs of NGC 6397, M15, and M30 presented in this paper come from the three WF chips combined; the CMD of M92 comes from the WF4 chip alone. The LFs have been obtained from the 3 WF chips for NGC 6397, from chip WF3 for M15 and M30, and from chip WF4 for M92. Adding the data from the other chips would marginally increase the statistical significance of the LFs. In view of the small error bars of the present LFs (see Fig. 2), we considered it not worth the large cpu time that would have been required to run the crowding experiments for every chip (see below).

In Figure 1 are the color–magnitude diagrams derived from this photometry. The diagram for NGC 6397 has been presented by CPK and is shown here for purposes of comparison. Detailed discussions of the other CMDs will appear elsewhere. Here we focus on the main-sequence luminosity functions derived from these CMDs. In all four cases we measure stars from the turnoff (or just below it) to a limiting magnitude  $V_{555}, V_{606} \gtrsim 27$ . The main sequence (MS) is well defined, spanning from 8 (M15) to nearly 10 magnitudes in  $V_{555}$  or  $V_{606}$ . All four MSs show characteristic bends, which are particularly important for best tuning the theoretical models (Alexander *et al.* 1996, and Section 4 of this paper). For  $V_{555}, V_{606} > 25$ , measurement errors cause the MS to broaden noticeably, but its ridge can be distinguished down to limiting magnitudes that correspond to an absolute magnitudes in the range  $M_{555} \sim 12\text{--}13$  for M15, M30, and M92 (see adopted distance moduli in Table 1). Only in the case of NGC 6397 does field contamination prevent a reliable identification of the faintest MS stars, below  $V_{555} \sim 26$ , which still corresponds to an absolute magnitude  $M_{555} \sim 14$  in this cluster.

Below and to the left of the main sequence in NGC 6397 is the cluster’s white dwarf cooling sequence (see CPK for a detailed description and analysis). No obvious white dwarfs are identifiable in the other three clusters (apart from one object at  $V = 24.6$  and  $V - I = -0.05$  in M15)—which is to be expected, since all have apparent distance moduli that are at least 2.3 magnitudes greater than NGC 6397.

Contamination by background and foreground stars is negligible for M15, M30, and M92, as expected from their galactic latitudes ( $|b| > 27^\circ$ ). By contrast, a large number of objects to the left and the right of the MS of NGC 6397 are background halo and foreground disk stars, respectively, the latter due to the cluster’s low latitude ( $b = -12^\circ$ ). Their numbers are in reasonable agreement with those predicted by the Bahcall & Soneira (1980) Galaxy model. In all four diagrams, at the faintest magnitudes there is probably also an admixture of unresolved galaxies.

Particular attention was devoted to determining the completeness of our samples. For each cluster we created 40 to 45 new images, using DAOPHOT (Stetson 1987, 1991). Each of these was the original image with up to 200 artificial stars added (no more, lest we alter the degree of

crowding). Each artificial star was a replica of the PSF, with Poisson noise added; the star was given a main-sequence color, and geometrical transformations were used to place it at the same randomly chosen position in both the  $V$  and the  $I$  image. The images containing artificial stars were measured in the same way as the original images. In the LFs presented here, we include only points for which the completeness figures were 50% or higher, so that none of the counts have been corrected by more than a factor of 2. For NGC 6397 and M30, the completeness is everywhere greater than 80%. The completeness drops below this level only in the last point of the M15 LF and in the last 3 points of the M92 LF.

The use of color–magnitude diagrams allows us to distinguish cluster stars from field stars. In three of the four clusters field contamination is very small, and this is an easy task: for M15, M30, and M92 the LF was obtained by counting stars within  $\pm 3$  sigmas of the MS ridge line, and otherwise ignoring field-star contamination. By contrast, Fig. 1 shows that the CMD of NGC 6397 suffers much interference from background and foreground stars. In this case we drew a main-sequence ridge line, read off its colors, and subtracted the corresponding main-sequence color from that of each star, so as to create a verticalized main sequence. As described in detail by CPK, we then drew lines on either side of the MS that excluded field stars, and corrected the regions between the lines for field-star contamination by using the star density in the neighboring regions outside them.

### 3. The Luminosity Functions

The LFs for the 4 clusters are shown in Fig. 2 and listed in Tables 2–5 with the completeness estimates. In Table 2–5, Col. 1 gives the  $V_{555}$  or  $V_{606}$  magnitudes, Col. 2 gives the completeness in the corresponding magnitude bin, and Col. 3 lists the actual counts, corrected for completeness and field contamination (where needed). The same figures for the  $I_{814}$  LFs are in Cols. 4–6. Fig. 2a shows the LFs from the  $I_{814}$  photometry, while Fig. 2b shows the  $V_{555}$  and  $V_{606}$  LFs; as the  $V_{555}$  and  $V_{606}$  magnitudes should differ by at most a few hundredths of a magnitude in the color

range covered by the CMDs in Fig. 1, a direct comparison of the  $V$  LFs is permissible. Adopted distance moduli are given in Table 1. The distance moduli and reddenings have been taken from the following papers: Piotto, Ortolani, & Zoccali (1996) for NGC 6397; Durrell & Harris (1993) for M15; Piotto *et al.* (1990) for M30; Stetson & Harris (1988) for M92. For NGC 6397, stars fainter than the turnoff were saturated even in our 60-sec exposures, so that the *HST*-based LF begins at  $I_{814} \sim 16.5$  ( $V_{555} \sim 17.1$ ). For this cluster, we extended the LFs upward to the turnoff using ground-based LFs obtained at a similar distance from the cluster center; for the  $I_{814}$  LF we used data from Drukier *et al.* (1993) and for the  $V_{555}$  LF data from Piotto *et al.* (1996). In both cases the *HST* and ground-based LFs agree well in the overlap regions (compare the filled triangles and open squares in Fig. 2a,b).

In the absence of a means of normalizing the four LFs to a global cluster parameter, arbitrary constants determine the vertical positioning of the individual LFs in Figs. 2a and 2b. We have chosen these constants in such a way as to align the four LFs at the bright end. Vertical shifts of the M30, M92, and NGC 6397 LFs were made to bring them into alignment with the M15 LF, according to a least-squares algorithm, in the magnitude intervals  $4 < M_{814} < 7$  and  $5 < M_{555} < 7.5$ . The shift adopted for NGC 6397 was determined from the *HST* measurements alone, but is further reinforced by the good match between the *HST* and ground-based measurements.

With the LFs aligned in this way, it can be seen that the  $I_{814}$ -band LFs of all clusters have a similar shape in the range  $4 \leq M_{814} \leq 7$ . At fainter magnitudes the LFs of M15, M30, and M92 continue to track one another closely, remaining similar over the entire range sampled, from the the turnoff down to  $M_{814} \simeq 10$ , or  $\mathcal{M} \sim 0.13\mathcal{M}_\odot$ . The NGC 6397 LF, by contrast, diverges downward for  $M_{814} \gtrsim 7$ , or  $M_{555} \gtrsim 8$  ( $\mathcal{M} \lesssim 0.5\mathcal{M}_\odot$ ), dropping below those of M15, M30, and M92 by as much as a factor of 2.5. A similar relative deficit of faint stars in NGC 6397 vs. M15, M30, and M92 is visible in the  $V_{555}$  LFs in Fig. 2b.

Had we chosen to align the NGC 6397 LF with the others at the faint instead of the bright end, the result would have been a relative excess of bright stars in NGC 6397. However, the range of magnitudes over which the NGC 6397 LF would be well-matched to the other three LFs would

in this case be somewhat smaller than when they are aligned at the bright end. Nevertheless, the present observations do not in themselves clearly distinguish between an excess of high-mass stars or a deficit of low-mass stars in this cluster, relative to the other three. But for reasons that will be discussed in Section 5 below, we will hereafter refer to the difference in the LFs as a deficit of faint stars in NGC 6397.

The difference between the NGC 6397 LF and the nearly identical LFs of M30, M15, and M92 is apparent only when they are compared over a large range of magnitudes. De Marchi & Paresce (1995) have asserted—incorrectly, as it turns out—that NGC 6397 and M15 have very similar LFs. This was the result of the shortness of the interval over which they compared their LFs—only  $M_{814} \simeq 6.5\text{--}10.1$ . Our *HST* LFs for NGC 6397 and M15 span a larger range of magnitudes, allowing a comparison from  $M_{814} \simeq 3.5\text{--}10.5$ . These LF measurements are in reasonable agreement with those of De Marchi & Paresce for M15, and with Paresce, De Marchi & Romaniello (1995) for NGC 6397, for the ranges in which we overlap with them; but the larger magnitude range that we measure shows that the two LFs have different shapes: that they match each other at the bright end, and that there is a marked deficiency of faint stars in NGC 6397 relative to M15 (as well as M30 and M92).

Before we can interpret the results of the LF comparison in Fig. 2, we must determine what corrections, if any, are required to convert these observed local LFs to global LFs. Our multimass model of NGC 6397 (King, Sosin, & Cool 1995) shows that the LF in its envelope differs little from the global LF, as mass-segregation effects, while strong, are largely confined to the small central regions. (The radial changes are shown in more detail in Figure 4 of King 1996.) To first order, these results are applicable to M15 and M30 as well, since all three clusters have collapsed cores (Djorgovski & King 1986) and similar surface-brightness profiles, and since the fields analyzed here are out in the envelopes in all three cases. More specifically, even with the small rescaling that is needed in fitting the NGC 6397 model to M15 and M30, their global MFs remain very close to the local MFs in the fields that we observed, differing nowhere by more than one or two tenths in the logarithm. As for M92, we have calculated multi-mass models of clusters of similar

central concentration. We find that whereas local mass functions at the center or very far out in the envelope differ considerably from the global one, at the intermediate radius at which we observed the local mass function is fortuitously quite close to the global one, with differences that again nowhere exceed one or two tenths in the logarithm. Thus in all four clusters our observed LFs are effectively global, and the large deficiency of faint stars in NGC 6397 is very unlikely to be due to differences between the local and global LFs.

#### 4. Mass Functions

Deep color–magnitude arrays also contain information about the low-mass-star content of clusters. But in order to extract this information, a transformation from luminosity to mass is required. As many authors have emphasized, such transformations remain uncertain for low-mass stars, especially for very-low-mass stars of low metal abundance. The transformation from an LF to an MF depends directly on the slope of the mass–luminosity relation (MLR), and different calculations of stellar models yield different slopes, particularly for the lowest-mass hydrogen-burning stars. To get a sense of the range of results that different MLRs produce, we have converted our LFs into MFs using several of those available in the literature (Bergbush and VandenBerg 1992, Baraffe *et al.* 1995, D’Antona & Mazzitelli 1995, Alexander *et al.* 1996). Caution must still be exercised in interpreting the resulting MFs, however, given the underlying problem of the paucity of observational constraints on any of these relations.

Of the existing models, we find that those of Alexander *et al.* (1996) reproduce the location of our main sequence in the CMD of NGC 6397 unusually well, as shown in Fig. 3. Not only is the overall fit of the isochrone from the model that has the metallicity of NGC 6397 satisfactory, from just below the turnoff to the very bottom of the observed main sequence, but also the distance modulus  $(m - M)_V = 12.4$  and the reddening  $E(V - I) = 0.19$  that result from the fit are in agreement, within the errors, with the distance and reddening of NGC 6397 found by Piotto *et al.* (1996) from an average of different methods. This result is somewhat reassuring, in the sense that

we can expect that if the models are able to predict the luminosities and temperatures, and also the corrections from the theoretical to the observational CMD plane, they should then be able also to predict the transformation from masses to absolute magnitudes, i.e., the MLR that we need. This does not mean that the MLR from the Alexander *et al.* (1996) models is the “correct” one; it is simply the best one presently available, and the cautionary remarks we made at the beginning of this section should still be heeded. The main sequences of M15, M30, and M92 all have very similar morphologies to that of NGC 6397. As a result, what has been said for the isochrone fitting of NGC 6397 also applies to the other three metal-poor clusters. To conclude, neither the D’Antona and Mazzitelli (1995) nor the Baraffe *et al.* (1995) isochrones reproduce the observed sequence of NGC 6397 as well as that of Alexander *et al.* However, for the sake of comparison, and to give an idea of the possible range of uncertainty, we will nevertheless use the MLR of D’Antona & Mazzitelli along with that of Alexander *et al.* in what follows. The former MLR produces the steepest MFs of any we tried, while the latter produces the shallowest MFs.

In Fig. 4 we compare the MFs derived from the  $I_{814}$  LF of NGC 6397 using both MLRs. The results are similar over most of the main sequence, from  $\mathcal{M} \simeq 0.8\text{--}0.15\mathcal{M}_\odot$ . But for the lowest-mass stars ( $\mathcal{M} \simeq 0.15\text{--}0.10\mathcal{M}_\odot$ ), the Alexander *et al.* MLR produces a MF that falls significantly below that produced by the D’Antona & Mazzitelli relation. This is a consequence of the steeper slope that the MLR of D’Antona & Mazzitelli has in this region.

Neither MF is particularly well fit by a power law over the entire mass range. For purposes of comparison with previous work, however, we have determined best-fit power laws for both MFs for masses below  $0.4\mathcal{M}_\odot$ . They are  $x = -0.1$  and  $x = 0.6$  for the MFs derived from Alexander *et al.* and D’Antona & Mazzitelli MLRs, respectively (where for the Salpeter law  $x = 1.35$ ). Neither is as steep as the  $x = 0.9$  slope determined by Fahlman *et al.* (1989) for this cluster. However that steep slope was derived from a correspondingly steep LF that disagrees with two independent sets of HST observations (see CPK). The discrepancy could be the result of inadequate correction for field stars in the ground-based study, a problem that we have already described as being critical for NGC 6397.

In Fig. 5 we compare the MFs derived from the  $I_{814}$  LF of M30, again using both the D’Antona & Mazzitelli and the Alexander *et al.* MLRs. Similar results are obtained for M15 and M92, since their LFs are so similar to that of M30. Again, neither MF is well fit by a single power law over the entire length of main sequence that is sampled. If the upper end of the main sequence is ignored, the MF derived using the D’Antona & Mazzitelli MLR can be reasonably well fit by a power law with slope  $x \sim 1$  for stars with  $\mathcal{M} < 0.4\mathcal{M}_\odot$ . The MF obtained using the Alexander *et al.* MLR is similar, but somewhat less well fit by a power law, even in this restricted range of masses. It shows some hint of flattening at the very-low-mass end, which is not seen in the MF that the D’Antona & Mazzitelli MLR produces. We emphasize that of the MLRs that we have tried, its ability to match our CMD makes the Alexander *et al.* MLR the one that is probably most reliable, though a direct comparison with observed masses will ultimately be needed.

## 5. Discussion

The primary finding of this study is that the main-sequence LFs and MFs of M15, M30, and M92 are almost as similar as they can be, while that of NGC 6397 is distinctly different. How are we to interpret this result?

The resemblance between M15, M30, and M92 would tend to suggest that these three clusters were born with similar MFs that have changed little since, or changed in similar ways. A scenario in which they were born different and have evolved to become the same seems too contrived. That NGC 6397 has a different LF may simply be an accident of birth. However, in view of the similarity between the other three clusters, it is interesting to ask whether the differences in NGC 6397 could be understood if all four clusters started out with similar mass functions, and evolved in different ways. Viewing the difference in the NGC 6397 LF as a relative deficit of low-mass stars, the answer—qualitatively, at least—is yes.

Of the more than 100 globular clusters for which physical parameters are given by Djorgovski (1993), NGC 6397 has the shortest central relaxation time; those of M15, M30, and M92 range

from one to three orders of magnitude longer. Also, among the 26 Galactic orbits given by Dauphole *et al.* (1996), NGC 6397 has one that is among the most vulnerable to tidal shocks; it oscillates rapidly through a dense part of the Galactic plane, only a few kiloparsecs from the Galactic center. By contrast, M15 has an orbit that subjects it very little to tidal shocks: it is much farther from the center, and slower moving (Dauphole *et al.* 1996). M92 may be an intermediate case; its orbit, which carries it quite close to the Galactic center at times, would make it vulnerable to shocks. However, this case is quite different from that of NGC 6397. Passages through the dense central part of the Galactic disk are much less frequent for M92, because its orbit is much more extended, and therefore has a much longer period. Moreover, the central relaxation time of M92 is so long that the possibility exists that the cluster has lost low-mass stars from its periphery but replenishes them so slowly from its inner parts that the loss no longer continues. However, the possibility that M92 has been affected by tidal shocks cannot be excluded. And we note that the faintest part of its LF does appear to fall somewhat below those of M15 and M30, though the difference is only at the 2-sigma level and is also affected by how we fit the curves together.

As no measurement of the proper motion of M30 exists, its Galactic orbit is poorly known; but its present distance from the Galactic plane and its radial velocity suggest that it has an orbit that is much less vulnerable to tidal shocks than is that of NGC 6397. The radial velocity of M30 is  $-186$  km/s, at  $(l, b) = (27^\circ, -47^\circ)$ . If its proper motion were zero, this radial velocity would indicate a speed, with respect to the Galactic center, of 240 km/s, sufficiently larger than circular to carry the cluster considerably farther from the Galactic center than its present distance of 6.8 kpc. While it is not beyond the realm of possibility that the unknown proper motion might reduce the magnitude of the cluster’s Galactocentric speed, the great majority of possible values of the proper motion would increase it. Thus M30 is most probably in an orbit much more like the low-shock orbit of M15 than the high-shock orbit of NGC 6397.

Both evaporation and losses via tidal shocking could be expected to have resulted in a depletion of low-mass stars in NGC 6397 relative to M15, M30, and M92. Moreover, the two effects should work in concert, with relaxation feeding low-mass stars to the cluster envelope as

fast as the tidal shocks remove them. We emphasize, however, that the rates of these effects are poorly known; detailed calculations of both the evaporation rate and the effects of tidal shocks on this cluster would be valuable. (Aguilar, Hut, & Ostriker [1988] carried out a study of these effects, showing their importance; but they treated the orbit of each cluster in a statistical way, for lack of knowledge—at that time—of actual orbits. A more recent study by Gnedin & Ostriker [1997], although more sophisticated in its approach, chose to ignore known orbits, “to maintain homogeneity of the sample”; they also treated orbits statistically.)

We further find that differences between existing MLRs for very-low-mass, metal-poor main-sequence stars are sufficient to produce noticeably different MFs from the same LF. The differences we find are greatest for NGC 6397, for which the LF that we measure reaches to the faintest absolute magnitudes. It remains unclear exactly how its MF behaves at the very-low-mass end. But the MF slopes that we find using any of the existing MLRs are shallower than the  $x = 1$  slope for which an integration of the total mass down to  $\mathcal{M} = 0$  would diverge. Thus, NGC 6397 appears not to contain a significant amount of mass in very-low-mass stars. At the same time, even the shallowest MF we obtained for NGC 6397 shows no sign of dropping, to the limit to which we can identify the main sequence. As for the bottom of the hydrogen-burning MS, it is clear that we have not yet reached it, as that region would manifest itself as a sharp drop-off in the LF.

M15, M30, and M92 all contain a larger fractional population of very-low-mass main-sequence stars than NGC 6397. For these three clusters, the best-fit power law for the MF at the low-mass end is close to the divergent slope of  $x = 1$  for stars with  $\mathcal{M} < 0.4\mathcal{M}_\odot$ . However, none of the MLRs we tried produced MFs for these clusters that are as steep as those reported for a small sample of other clusters by Richer *et al.* (1991). Furthermore, since most of the MLRs we tried produced MFs that begin to flatten out near the low-mass limit of our measurements, we conclude that the MFs probably do not rise so fast as to make the low-mass end dominant. It is important to emphasize, however, that globular-cluster MFs will remain uncertain until the mass–luminosity relation for very-low-mass, low-metallicity stars is better determined. Fortunately, such uncertainties do not affect comparisons between clusters with similar metallicities, and much progress in that area can

be anticipated in the near future.

We thank F. D'Antona, V. Castellani, S. Cassisi, and E. Brocato for providing isochrones in advance of publication, D. Vandenberg for providing a computer-readable version of his isochrones, and P. Stetson for his generosity with software. We also note that the M15 data used here exists as a result of the foresight of E. Groth in setting up a parallel-observing program for HST. This work was supported by NASA Grant NAG5-1607. GP acknowledges partial support by the Consiglio Nazionale delle Ricerche and by the Agenzia Spaziale Italiana.

## REFERENCES

Alexander, D. R., Brocato, E., Cassisi, S., Castellani, V., Ciacio, F., & Degl'Innocenti, S. 1996, A&A, submitted

Anderson, J., King, I. R., & Sosin, C. 1995, in Calibrating HST: Post Servicing Mission, eds. A. Koratkar & C. Leitherer (Baltimore: STScI), p. 300

Aguilar, L., Hut, P., & Ostriker, J. P. 1988, ApJ, 335, 720

Bahcall, J. M., & Soneira, R. M. 1980, ApJS, 66, 73

Baraffe, I., Chabrier, G., Allard, F., & Hauschildt, P.H. 1995, ApJ, 446, L35

Bergbusch, P. A., & VandenBerg, D. A. 1992, ApJS, 81, 163

Brocato, E., Cassisi, S., Castellani, V., Cool, A. M., King, I. R., & Piotto, G. 1996, in Formation of the Galactic Halo....Inside and Out, eds. H. Morrison & A. Sarajedini (San Francisco: ASP), p. 76

Cool, A. M., & King, I. R. 1995, in Calibrating HST: Post Servicing Mission, eds. A. Koratkar & C. Leitherer (Baltimore: STScI), p. 290

Cool, A. M., Piotto, G., & King, I. R. 1996, ApJ, 468, 655 (CPK)

D'Antona, F. & Mazzitelli, I. 1995, ApJ, 456, 329

Dauphole, B., Geffert, M., Colin, J., Ducourant, C., Odenkirchen, M., & Tucholke, H.-J. 1996, A&A, in press

De Marchi, G., & Paresce, F., 1995, A&A, 304, 202

Djorgovski, S. 1993, in Structure and Dynamics of Globular Clusters, eds. S. G. Djorgovski & G. Meylan (San Francisco: ASP), p. 373

Djorgovski, S., & King, I. R. 1986, ApJ, 305, L61

Djorgovski, S., Piotto, G., & Capaccioli, M. 1993, AJ, 105, 2148

Drukier, G. A., Fahlman, G. G., Richer, H. B., Searle, L., & Thompson, I. 1993, AJ, 106, 2335

Durrell, P. R., & Harris, W. E. 1993, AJ, 105, 1420

Fahlman, G. G., Richer, H. B., Searle, L., & Thompson, I. B. 1989, ApJ, 343, L49

Gnedin, O. Y., & Ostriker, J. P. 1997, preprint astro-ph/9603042

Holtzman, J. A., Burrows, C. J., Casertano, S., Hester, J. J., Watson, A. M., & Worthey, G. S. 1995, PASP, 107, 1065

King, I. R. 1996, in *Dynamical Evolution of Star Clusters*, eds. P. Hut & J. Makino (Dordrecht: Kluwer), p. 29

King, I. R., Sosin, C., & Cool, A. M. 1995, ApJL, 452, L33

McClure, R. D., VandenBerg, D. A., Smith, G. H., Fahlman, G. G., Richer, H. B., Hesser, J. E., Harris, W. E., Stetson, P. B., & Bell, R. A. 1986, ApJ, 307, L49

Paresce, F., De Marchi, G., & Romaniello, M. 1995, ApJ, 440, 216

Piotto, G., Ortolani, S., & Zoccali, M. 1996, submitted to A&A

Reid, I. N., Yan, L., Majewski, S., Thompson, I., & Smail, I. 1996, AJ, 112, 1472

Richer, H. B., Fahlman, G. G., Buonanno, R., Fusi Pecci, F., Searle, L., & Thompson, I. B. 1991, ApJ, 381, 147

Richer, H. B., & Fahlman, G. G. 1992, Nature, 358, 383

Stetson, P. B. 1987, PASP, 99, 101

Stetson, P. B. 1991, in *ESO/ST-ECF Data Analysis Workshop*, eds. P. J. Grosbøl and R. H. Warmels, ESO Conf. and Workshop Proc. No. 38 (Garching: ESO), p. 187

Fig. 1—  $(V, V - I)$  color-magnitude diagrams of M15 (NGC 7078), M30 (NGC 7099), M92 (NGC 6341), and NGC 6397. Note that two different  $V$  filters were used.

Fig. 2a—  $M_{814}$  LFs for NGC 6397, M15, M30, and M92. The LF for NGC 6397 has been extended up to the turnoff using ground-based data. Note the similarity between the  $M_{814}$  LFs for M15, M30, and M92, and the significantly shallower slope of the LF for NGC 6397 relative to those of the other three clusters.

Fig. 2b—  $M_V$  LFs for NGC 6397, M15, M30, and M92. The LF for NGC 6397 has been extended up to the turnoff using ground-based data. As in Fig. 2a, note the similarity between the  $M_V$  LFs for M15, M30, and M92, and the significantly shallower slope of the LF for NGC 6397 relative to those of the other three clusters.

Fig. 3— Comparison of our NGC 6397 CMD with theoretical curves from Alexander *et al.* (1996).

Fig. 4— Mass functions for NGC 6397, converted from the  $I_{814}$  LFs shown in Fig. 1, using the MLRs from Alexander *et al.* (1996) (solid line) and from D'Antona & Mazzitelli (1995) (dotted line). Three specific masses referred to in the text are marked with arrows.

Fig. 5— Same as Fig. 4, but for M30 (NGC 7099).

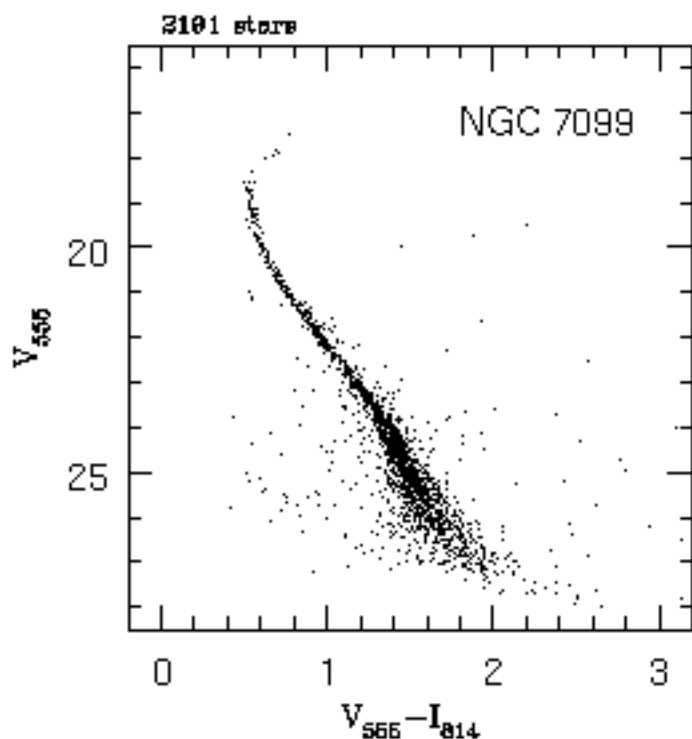
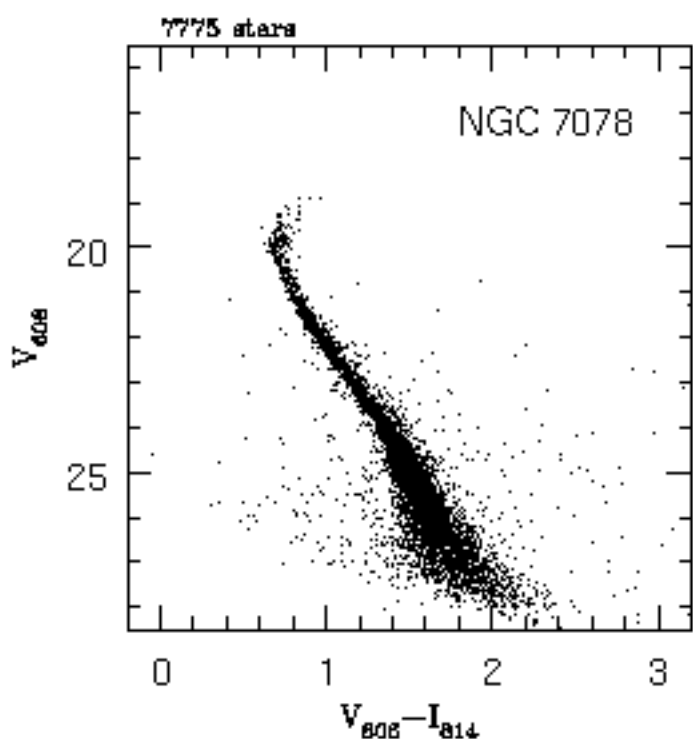
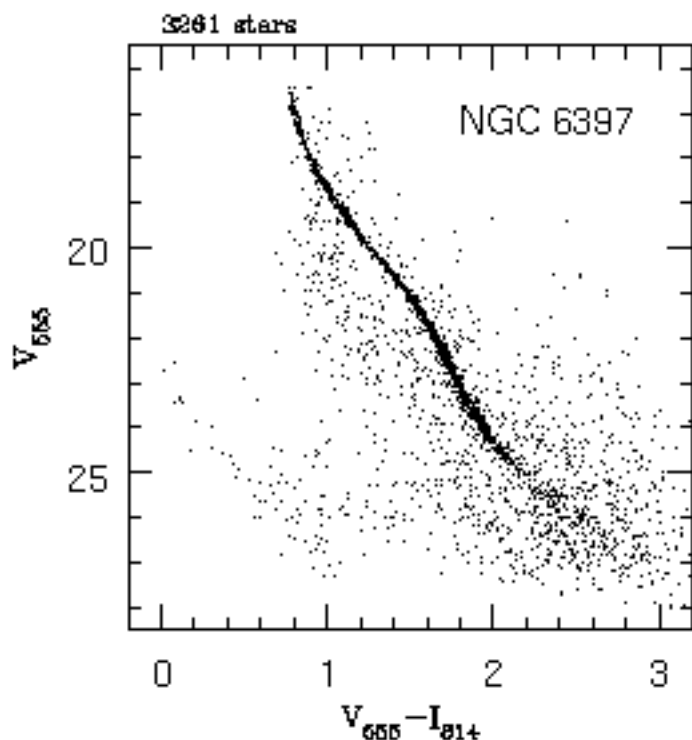
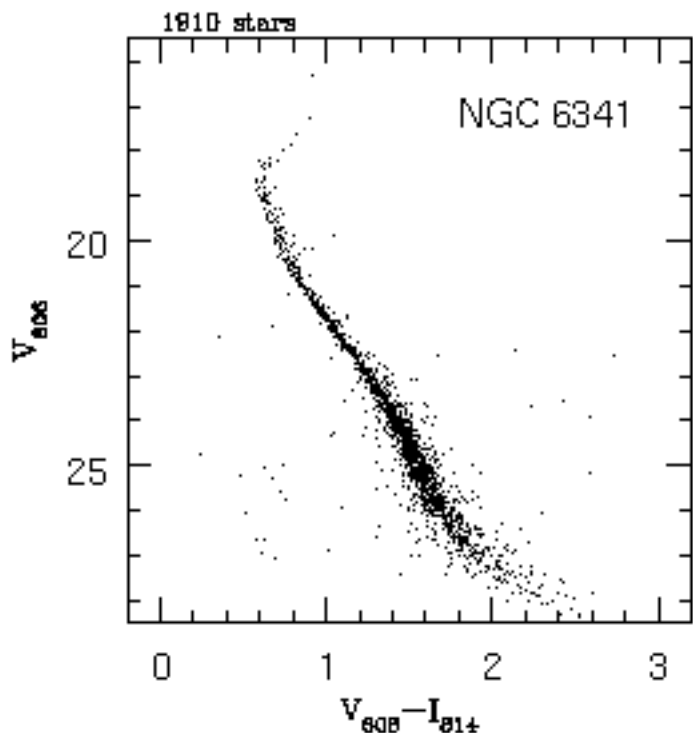
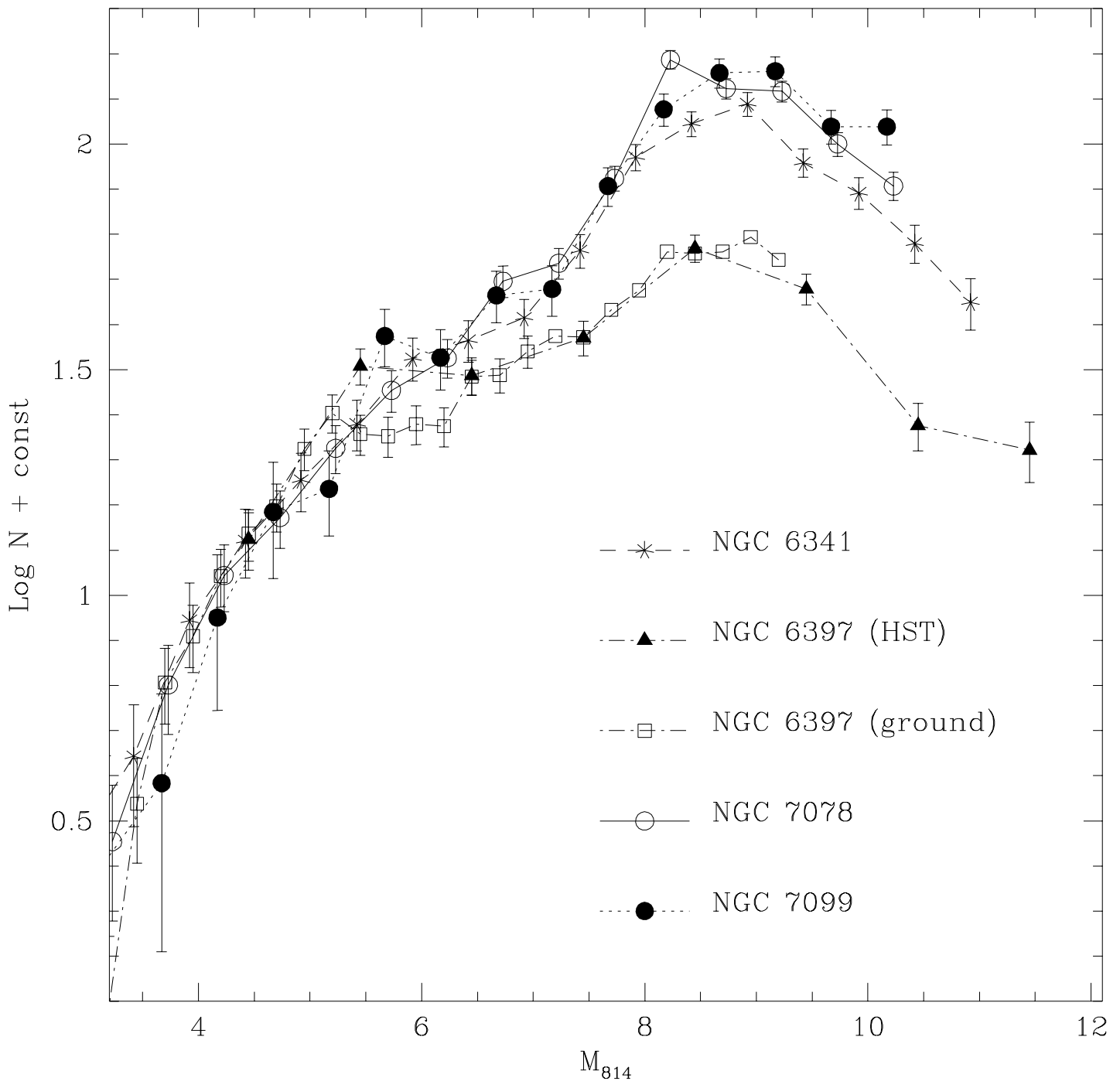


TABLE 1. Data Sets

Cluster	[Fe/H]	$(m - M)_I$	$(m - M)_V$	Dates	Filter	$t_{\text{exp}}(\text{sec})$
NGC 6341	-2.2	14.58	14.60	Dec 5,15 1995	F606W	8275
					F814W	8275
NGC 6397	-1.9	12.05	12.30	Aug 19,20 1994; Oct 18 1994	F555W	14200
					F814W	18700
NGC 7078	-2.2	15.26	15.40	June 17,18 1994	F606W	6050
					F814W	6050
NGC 7099	-2.1	14.48	14.65	Dec 5-8 1994	F555W	15300
					F814W	8700



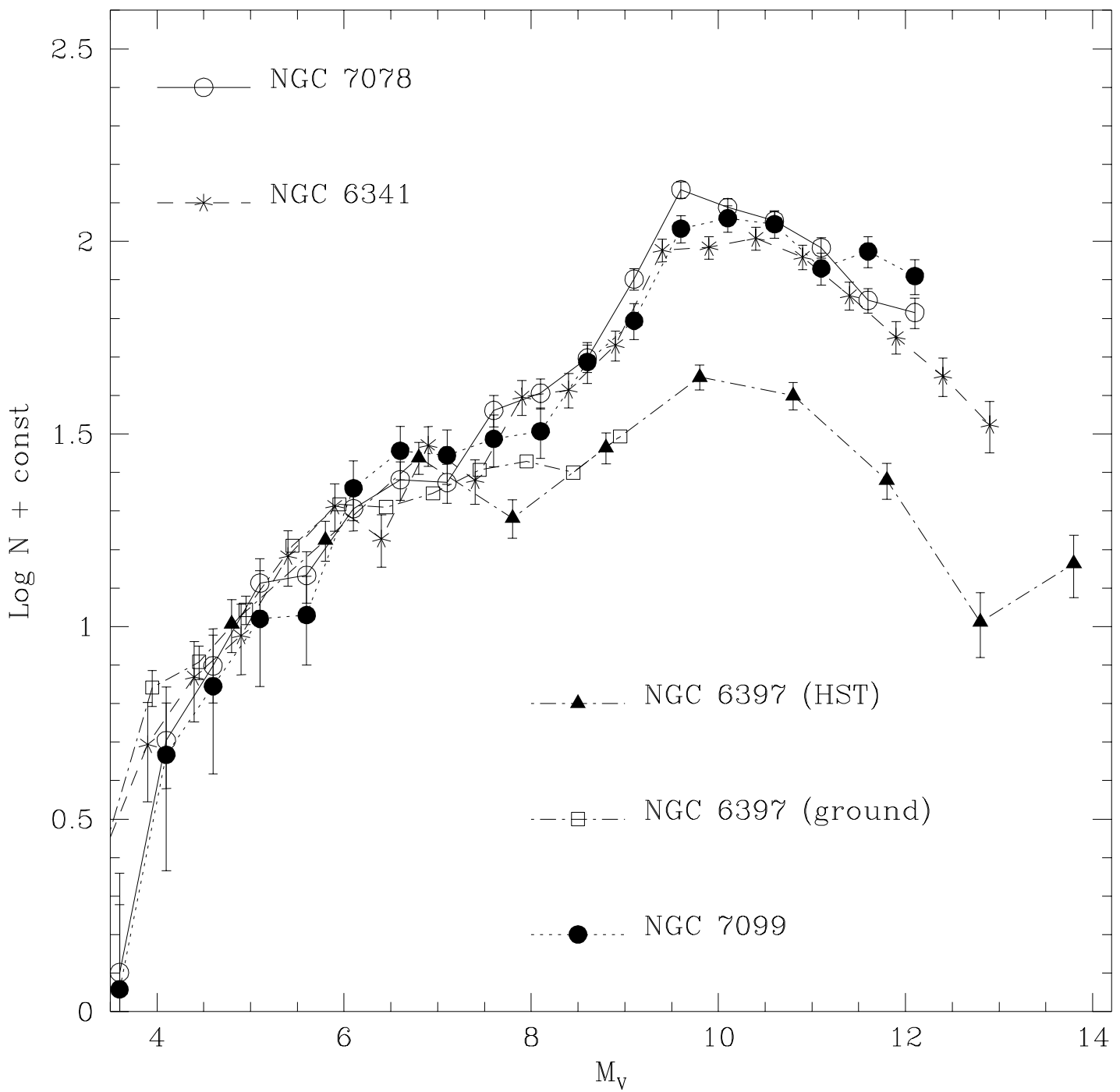


TABLE 2. NGC 6341

$V_{606}$	Compl	$LF_V$	$I_{814}$	Compl	$LF_I$
17.00	1.00	1.0	16.50	1.00	2.0
17.50	1.00	2.0	17.00	1.00	4.0
18.00	1.00	6.0	17.50	1.00	7.0
18.50	1.00	12.0	18.00	1.00	11.0
19.00	1.00	18.0	18.50	1.00	22.0
19.50	1.00	23.0	19.00	1.00	33.0
20.00	1.00	37.0	19.50	1.00	45.0
20.50	1.00	50.0	20.00	1.00	60.0
21.00	1.00	41.0	20.50	0.99	83.8
21.50	0.99	71.8	21.00	0.98	91.8
22.00	0.98	58.2	21.50	0.97	103.0
22.50	0.97	95.9	22.00	0.95	145.2
23.00	0.96	100.0	22.50	0.94	233.9
23.50	0.95	130.6	23.00	0.93	277.3
24.00	0.94	230.7	23.50	0.87	306.9
24.50	0.93	234.4	24.00	0.84	227.5
25.00	0.88	247.7	24.50	0.79	195.0
25.50	0.85	221.3	25.00	0.71	150.7
26.00	0.82	175.8	25.50	0.53	111.4
26.50	0.78	137.1			
27.00	0.69	108.6			
27.50	0.53	81.1			

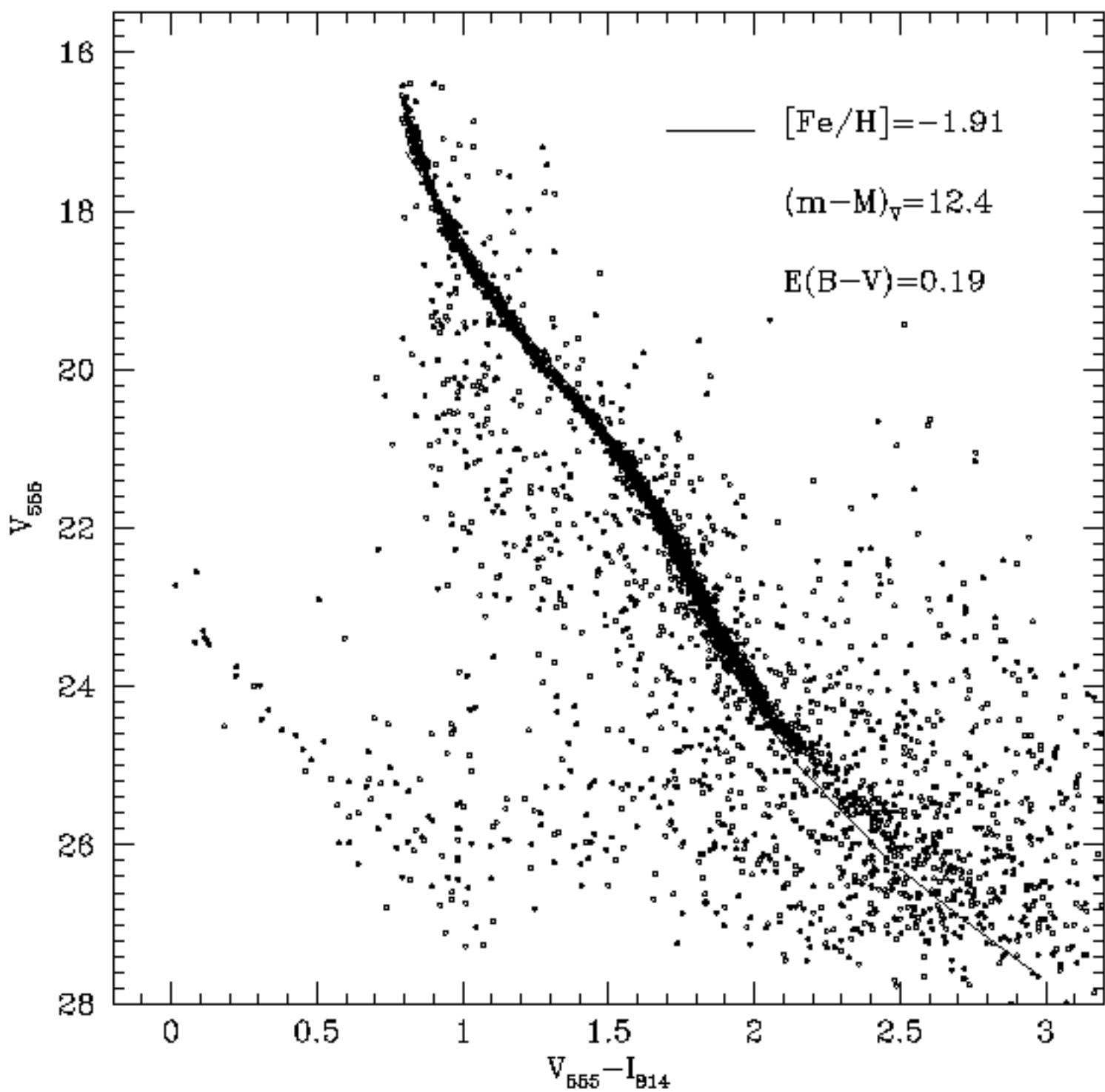


TABLE 3. NGC 6397

$V_{555}$	Compl	$LF_V$	$I_{814}$	Compl	$LF_I$
17.10	1.00	43.3	16.5	1.00	49.82
18.10	1.00	71.7	17.5	1.00	120.5
19.10	1.00	117.1	18.5	1.00	114.8
20.10	1.00	81.6	19.5	0.98	136.6
21.10	0.98	122.0	20.5	0.97	213.3
22.10	0.97	183.8	21.5	0.96	171.6
23.10	0.91	156.3	22.5	0.93	82.74
24.10	0.91	96.2	23.5	0.90	70.71
25.10	0.92	40.0			
26.10	0.86	53.6			

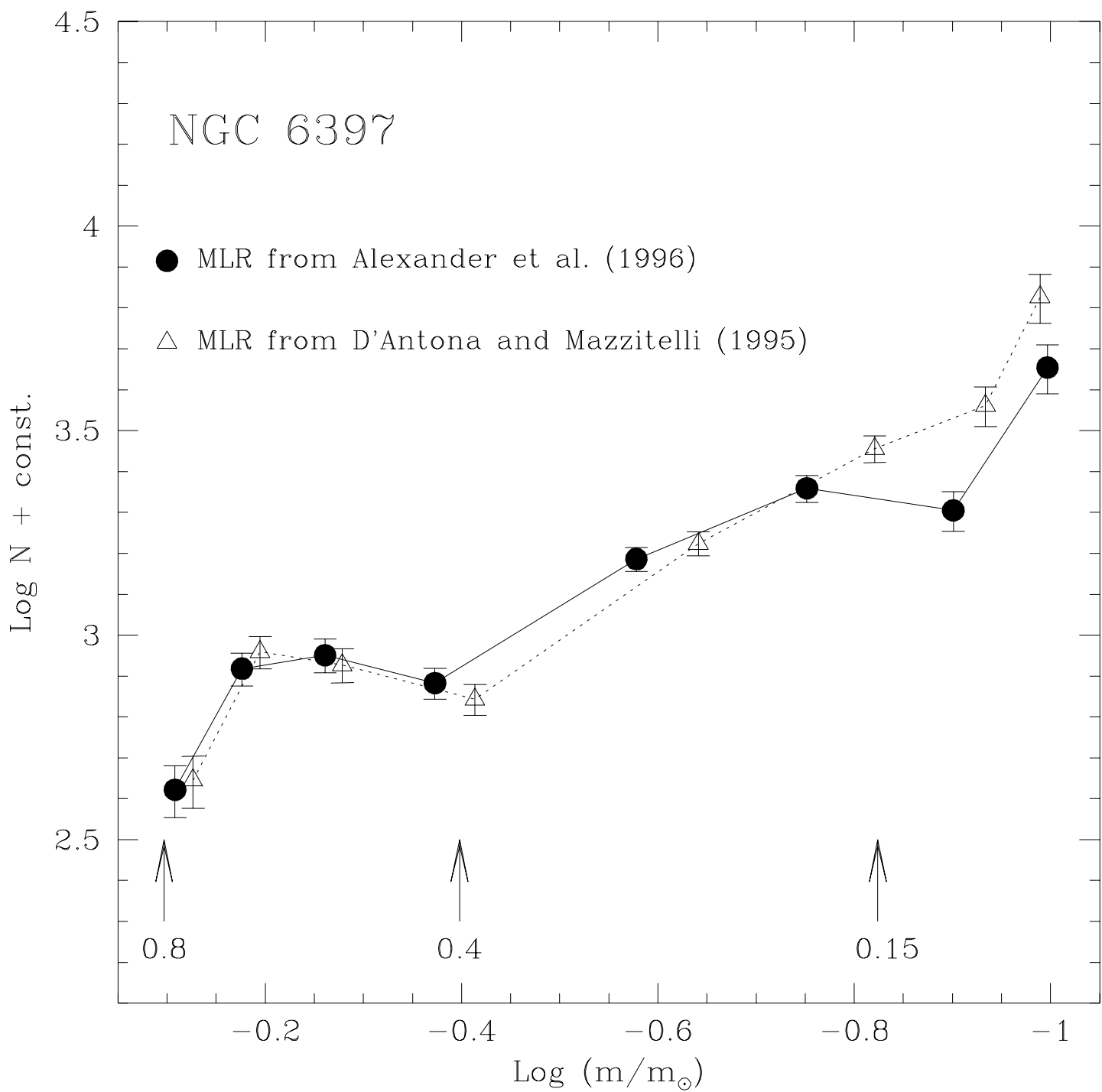


TABLE 4. NGC 7078

$V_{606}$	Compl	$LF_V$	$I_{814}$	Compl	$LF_I$
19.00	1.00	4.0	18.50	1.00	9.0
19.50	1.00	16.0	19.00	1.00	20.0
20.00	1.00	25.0	19.50	1.00	35.0
20.50	1.00	41.0	20.00	1.00	47.0
21.00	1.00	43.0	20.50	1.00	67.0
21.50	1.00	64.0	21.00	1.00	89.9
22.00	1.00	76.0	21.50	0.99	106.2
22.50	0.99	74.8	22.00	0.98	157.0
23.00	0.99	115.1	22.50	0.97	172.2
23.50	0.98	127.6	23.00	0.96	265.5
24.00	0.96	157.4	23.50	0.94	486.4
24.50	0.96	252.3	24.00	0.92	419.8
25.00	0.93	430.5	24.50	0.87	414.0
25.50	0.92	387.3	25.00	0.87	316.2
26.00	0.89	358.1	25.50	0.76	255.3
26.50	0.86	304.8			
27.00	0.85	222.3			
27.50	0.60	206.5			

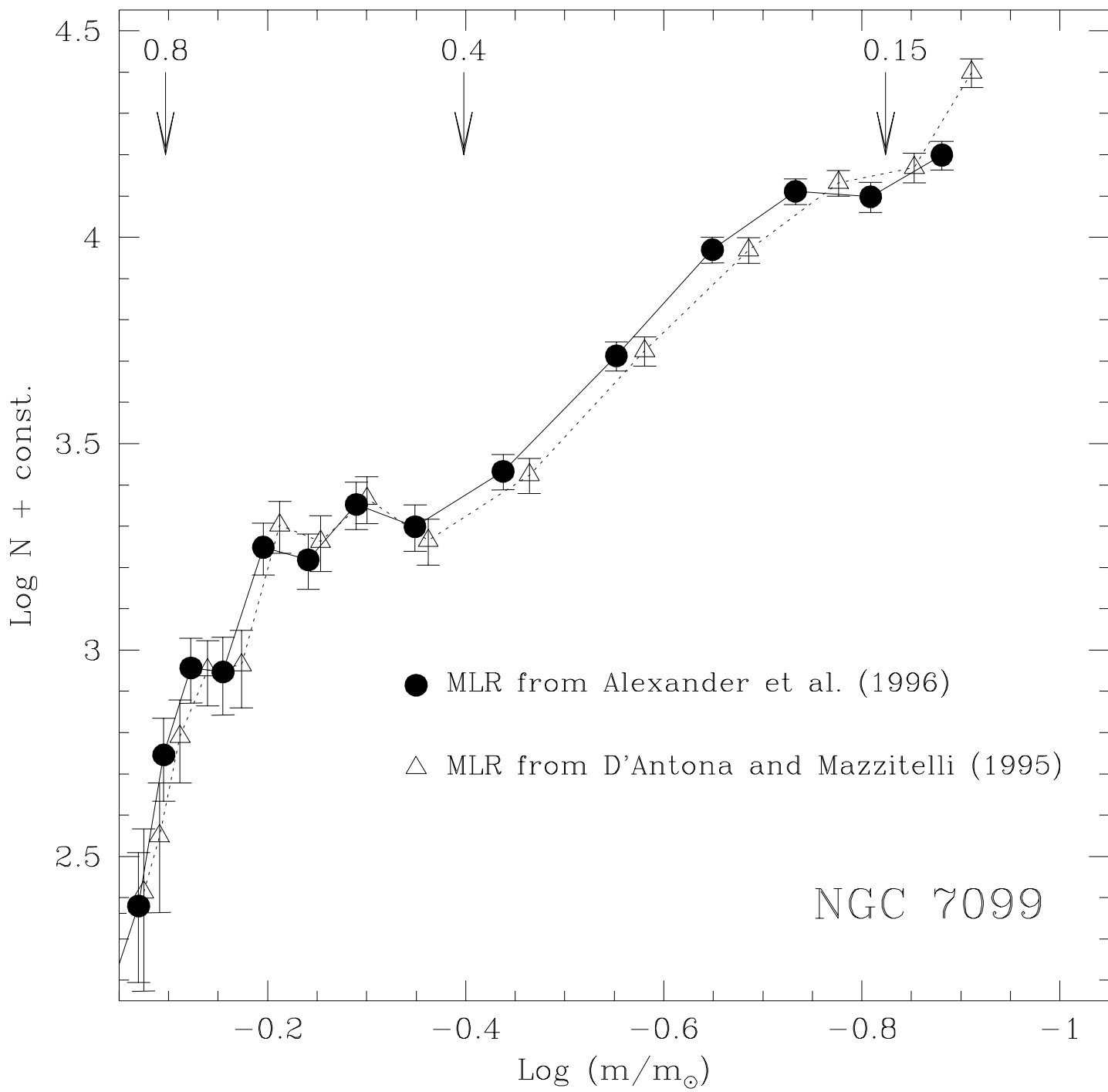


TABLE 5. NGC 7099

$V_{555}$	Compl	$LF_V$	$I_{814}$	Compl	$LF_I$
18.25	0.89	1.8	17.75	1.00	3.3
18.75	1.00	6.5	18.25	1.00	4.9
19.25	1.00	9.8	18.75	1.00	11.4
19.75	1.00	14.7	19.25	1.00	19.6
20.25	1.00	15.0	19.75	1.00	22.0
20.75	1.00	32.0	20.25	1.00	48.0
21.25	1.00	40.0	20.75	1.00	43.0
21.75	1.00	39.0	21.25	1.00	59.0
22.25	1.00	43.0	21.75	1.00	61.0
22.75	1.00	45.0	22.25	1.00	103.0
23.25	1.00	68.0	22.75	0.99	152.5
23.75	1.00	87.0	23.25	0.97	183.5
24.25	0.98	151.0	23.75	0.96	185.4
24.75	0.97	160.8	24.25	0.93	144.1
25.25	0.96	155.2	24.75	0.88	139.8
25.75	0.94	119.1			
26.25	0.91	131.9			
26.75	0.80	113.8			